Model based identification of aging parameters in lithium ion batteries

Githin K. Prasad*, Christopher D. Rahn*

Department of Mechanical and Nuclear Engineering, Pennsylvania State University, University Park 16802, United States

HIGHLIGHTS

▶ Developed a control oriented single particle model for a Li-ion battery.
▶ Developed least squares and recursive parameter estimators for SOH estimation.
▶ Observed a monotonic increase in the estimates of resistance and diffusion time.
▶ Correlated the parameter variations to aging mechanisms such as SEI layer growth.

ARTICLE INFO

ABSTRACT

As lithium ion cells age, they experience power and energy fade associated with impedance rise and capacity loss, respectively. Identification of key aging parameters in lithium ion battery models can validate degradation hypotheses and provide a foundation for State of Health (SOH) estimation. This paper develops and simplifies an electrochemical model that depends on two key aging parameters, cell resistance and the solid phase diffusion time of Li$^+$ species in the positive electrode. Off-line linear least squares and on-line adaptive gradient update processing of voltage and current data from fresh and aged lithium ion cells produce estimates of these aging parameters. These estimated parameters vary monotonically with age, consistent with accepted degradation mechanisms such as solid electrolyte interface (SEI) layer growth and contact loss.

© 2013 Elsevier B.V. All rights reserved.

1. Introduction

Hybrid and electric vehicles can contribute to a greener and cleaner environment by substantially reducing the dependance on non-renewable fossil fuels such as gasoline and diesel. Lithium ion batteries are widely used for energy storage in these vehicles mainly due to their high power and energy density. Hybrid electric vehicles have repeated charge and discharge cycles which deteriorate the battery due to irreversible physical and chemical degradation. State of health (SOH) in a lithium ion battery is typically defined as the ratio of the current capacity over the nominal capacity of a fresh battery and monotonically decreases as the battery ages. Impedance also rises as a battery ages, decreasing the maximum power output and efficiency.

Researchers have extensively studied capacity and power fade in lithium ion batteries [1–3]. Power fade is primarily due to an increase in internal resistance or impedance. Internal resistance

causes ohmic losses that waste energy, produce heat, and accelerate aging. Lithium ion batteries lose capacity over time due to degradation of the positive and negative electrodes and the electrolyte. The degradation mechanisms are complex, coupled, and dependant on cell chemistry, design, and manufacturer [4].

Considerable effort has been put into the development of high fidelity battery models that accurately predict voltage given the input current and model parameters [5,6]. The model parameters that provide the best match between the model predicted and experimentally measured voltage change with age. The change in system parameters due to aging depends on the degradation mechanism in a given cell. If the predominant degradation mechanism can be determined then the parameters that are most closely associated with that mechanism would be most likely to change. If the degradation mechanism involves unmodeled dynamics in the cell, however, then the correlation between the mechanism and system parameters becomes unclear.

Ramadass et al. [3] link cell aging to the change of only a few parameters in an electrochemical battery model. For a lithium ion cell, they find that the solid electrolyte film resistance and the solid state

* Corresponding authors.
    E-mail addresses: gkp104@psu.edu, githinprasad@gmail.com (G.K. Prasad), cdrahn@psu.edu (C.D. Rahn).

diffusion coefficient of the anodic active material are linked to cell degradation. Schmidt et al. [7] find that electrolyte conductivity and cathodic porosity are key parameters to estimate the rate capability fade and the capacity loss of a Li-ion cell. Zhang et al. [8] characterize the cycle life of lithium ion batteries with LiNiO$_2$ cathode and conclude that the impedance rise and capacity fade during cycling are primarily caused by the positive electrode. A solid electrolyte interface (SEI) layer forms on the positive electrode and it thickens and changes properties during cycling, causing a cell impedance rise and power fade.

Parameter estimation techniques based on equivalent circuit models have been developed to quantify the degradation in lithium ion batteries. Remmlinger et al. [9] monitor the state of health of lithium ion batteries in electric vehicles using an onboard internal resistance estimation technique. Kalman filters [10–14] have been developed to estimate the SOH using the equivalent circuit models. Troltzsch et al. [15] characterize aging effects in lithium ion batteries using impedance spectroscopy. Kim et al. [16] implement a dual sliding mode observer to estimate the capacity fade in lithium ion batteries.

In this paper, we estimate the SOH of a lithium ion battery based on a control oriented single particle model that explicitly relates the coefficients of the Padé approximated transfer function to the fundamental physical parameters of the battery. Two key composite parameters, the cell resistance and the diffusion time of the Li$^+$ species in the positive electrode are estimated based on voltage and current data from batteries that have been aged using a 5C rate cycle. The parameter variation with age is correlated to capacity loss and specific degradation mechanisms. The identified parameters act as SOH indicators if they can be shown to vary monotonically as the battery degrades.

2. Control oriented single particle model

A lithium ion cell consists of three domains: A negative composite electrode, a separator, and a positive composite electrode as shown in Fig. 1. Lithium metal oxide (LiMO$_2$) and lithiated carbon (Li$_x$C) are the active materials in the positive and negative electrodes, respectively. The metal in the positive electrode is a transition metal, typically Co. The active materials are bonded to metal foil current collectors at both ends of the cell and electrically insulated by a microporous polymer separator film or gel-polymer. Liquid or gel-polymer electrolytes enable lithium ions (Li$^+$) to diffuse between the positive and negative electrodes. The lithium ions insert into or deinsert from the active materials via an intercalation process. The insulating separator forces electrons to follow an opposite path through an external circuit or load.

The single particle (SP) model used in this paper assumes a single electrode particle in each electrode and negligible electrolyte diffusion and is detailed in [17]. The governing equations, transcendental transfer functions, and Padé approximation are summarized here for completeness.

Conservation of Li$^+$ species in a single spherical active material particle is described by Fick's law of diffusion,

$$\frac{\partial c_s}{\partial t} = \frac{D_s}{r^2}\frac{\partial}{\partial r}\left(r^2\frac{\partial c_s}{\partial r}\right) \quad \text{for } r \in (0, R_s), \tag{1}$$

where $r \in (0, R_s)$ is the radial coordinate, R_s is the particle radius, $c_s(r,t)$ is the concentration of Li$^+$ ions in the particle as a function of radial position r and time t, and D_s is the solid phase diffusion coefficient. We use the subscripts s and s, e to indicate solid phase and solid/electrolyte interface, respectively. The boundary conditions are

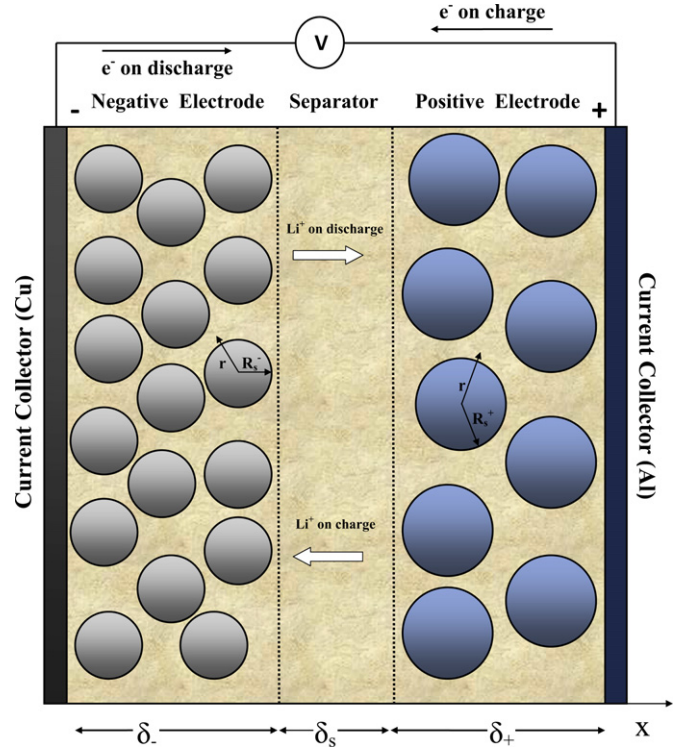$$\left.\frac{\partial c_s}{\partial r}\right|_{r=0} = 0, \tag{2}$$

Fig. 1. 1D schematic of the lithium ion battery model.

$$\left.D_s\frac{\partial c_s}{\partial r}\right|_{r=R_s} = -\frac{j}{a_s F}, \tag{3}$$

where $j(x, t)$ is the rate of electrochemical reaction at the particle surface (with $j > 0$ indicating ion discharge), F is Faraday's constant (96487 C mol^{-1}), and a_s is the specific interfacial surface area. For the spherical active material particles occupying electrode volume fraction ε_s, $a_s = 3\varepsilon_s/R_s$. The linearized Butler–Volmer electrochemical kinetics is given by

$$\eta = \frac{R_{ct}}{a_s}j \tag{4}$$

where the overpotential η drives the current flow across the electrode/electrolyte interface, $R_{ct} = RT/i_0 F(\alpha_a + \alpha_c)$ is the charge transfer resistance, i_0 is the exchange current density, R is the universal gas constant, T is the temperature, and α_a and α_c are the anodic and cathodic transfer coefficients, respectively.

The final transcendental impedance transfer function is given by

$$\begin{aligned}
\frac{V(s)}{I(s)} = &-\frac{R_{ct_+}}{a_{s_+}}\frac{1}{A\delta_+} - \frac{R_{ct_-}}{a_{s_-}}\frac{1}{A\delta_-} \\
&- \frac{\partial U^+}{\partial c_{s,e+}}\frac{1}{A\delta_+}\frac{R_s}{a_{s+}FD_{s+}}\left[\frac{\tanh(\beta_+)}{\tanh(\beta_+)-\beta_+}\right] \\
&- \frac{\partial U^-}{\partial c_{s,e-}}\frac{1}{A\delta_-}\frac{R_s}{a_{s-}FD_{s-}}\left[\frac{\tanh(\beta_-)}{\tanh(\beta_-)-\beta_-}\right] - \frac{R_f}{A}
\end{aligned} \tag{5}$$

where the electrode open circuit potentials U are linearized with the assumed constant slope $\partial U/\partial c_{s,e}$, $\beta = R_s\sqrt{s/D_s}$ with s the Laplace variable, δ is the thickness of the electrode, R_f is the contact resistance associated with physical connections to the cell and A is the cell surface area.

The infinite dimensional single particle model in Eq. (5) is discretized by a Padé Approximation [17,18]. A third order Padé approximation is generated for each particle transfer function resulting in the impedance transfer function

$$Z(s) = R_T + \frac{b_2 s^2 + b_1 s + b_0}{s^3 + a_2 s^2 + a_1 s} + \frac{d_2 s^2 + d_1 s + d_0}{s^3 + c_2 s^2 + c_1 s} \qquad (6)$$

where the numerator and denominator coefficients are shown in Table 1 with

$$Z(s) = \frac{R_T^+ s^3 + \left(21\,\mathscr{C}^+ + 189\dfrac{R_T^+}{\tau_D^+}\right)s^2 + \left(1260\dfrac{\mathscr{C}^+}{\tau_D^+} + 3465\dfrac{R_T^+}{\tau_D^{+2}}\right)s + 10395\dfrac{\mathscr{C}^+}{\tau_D^{+2}}}{s^3 + \dfrac{189}{\tau_D^+}s^2 + \dfrac{3465}{\tau_D^{+2}}s}. \qquad (9)$$

$$C_+ = \frac{\partial U^+}{\partial c_{s,e+}}, \quad C_- = \frac{\partial U^-}{\partial c_{s,e-}} \qquad (7)$$

Eq. (6) can be rewritten as

$$
\begin{aligned}
Z(s) = R_T &+ \frac{21\,\mathscr{C}^+ s^2 + 1260\dfrac{\mathscr{C}^+}{\tau_D^+}s + 10395\dfrac{\mathscr{C}^+}{\tau_D^{+2}}}{s^3 + \dfrac{189}{\tau_D^+}s^2 + \dfrac{3465}{\tau_D^{+2}}s} \\
&+ \frac{21\,\mathscr{C}^- s^2 + 1260\dfrac{\mathscr{C}^-}{\tau_D^-}s + 10395\dfrac{\mathscr{C}^-}{\tau_D^{-2}}}{s^3 + \dfrac{189}{\tau_D^-}s^2 + \dfrac{3465}{\tau_D^{-2}}s}.
\end{aligned}
\qquad (8)
$$

The simplified transfer function Eq. (8) depends only on five independent parameters

$$R_T = -\frac{R_{ct_+}}{a_{s_+}}\frac{1}{A\delta_+} - \frac{R_{ct_-}}{a_{s_-}}\frac{1}{A\delta_-} - \frac{R_f}{A}$$

$$\mathscr{C}^+ = \frac{C_+}{AFa_{s+}\delta_+ R_s^+} = \frac{C_+}{3AF\delta_+\varepsilon_{s+}}$$

$$\tau_D^+ = \frac{[R_{s+}]^2}{D_{s+}}$$

$$\mathscr{C}^- = \frac{C_-}{AFa_{s-}\delta_- R_{s-}} = \frac{C_-}{3AF\delta_-\varepsilon_{s-}}$$

$$\tau_D^- = \frac{[R_{s-}]^2}{D_{s-}}.$$

Table 1
Coefficient values.

Numerator	Value	Denominator	Value
b_0	$10395 C_+ [D_{s+}]^2/AFa_{s+}\delta_+[R_{s+}]^5$	a_0	0
b_1	$1260 C_+ D_{s+}/AFa_{s+}\delta_+[R_{s+}]^3$	a_1	$3465[D_{s+}]^2/[R_{s+}]^4$
b_2	$21 C_+/AFa_{s+}\delta_+ R_{s+}$	a_2	$189 D_{s+}/[R_{s+}]^2$
d_0	$10395 C_- [D_{s-}]^2/AFa_{s-}\delta_-[R_{s-}]^5$	c_0	0
d_1	$1260 C_- D_{s-}/AFa_{s-}\delta_-[R_{s-}]^3$	c_1	$3465[D_{s-}]^2/[R_{s-}]^4$
d_2	$21 C_-/AFa_{s-}\delta_- R_{s-}$	c_2	$189 D_{s-}/[R_{s-}]^2$

The total resistance of the battery R_T results from the contact resistance and the charge transfer resistance in both electrodes. The capacity factors $\mathscr{C}$ are inversely proportional to the electrode volume fraction and directly proportional to the slope $\partial U/\partial c_{s,e}$. The diffusion times τ_D is directly proportional to the square of the particle radius and inversely proportional to the solid phase diffusion coefficient.

The single particle model is further simplified by neglecting the impedance of the negative electrode. This assumption is validated by comparing the frequency responses as shown in Fig. 2. The positive electrode model closely matches the original SP model over the entire frequency range.

The simplified transfer function

depends only on the three composite parameters R_T^+ (neglecting the charge transfer resistance of the negative electrode), $\mathscr{C}^+$ and τ_D^+ which can be estimated from experimental data and hence can be used to monitor the state of health of the battery.

3. Least squares parameter estimation algorithm

Using voltage measurements over a sufficiently long time and with persistently exciting current input, a least squares technique can used to identify the coefficients of the transfer function Eq. (9) which has the form

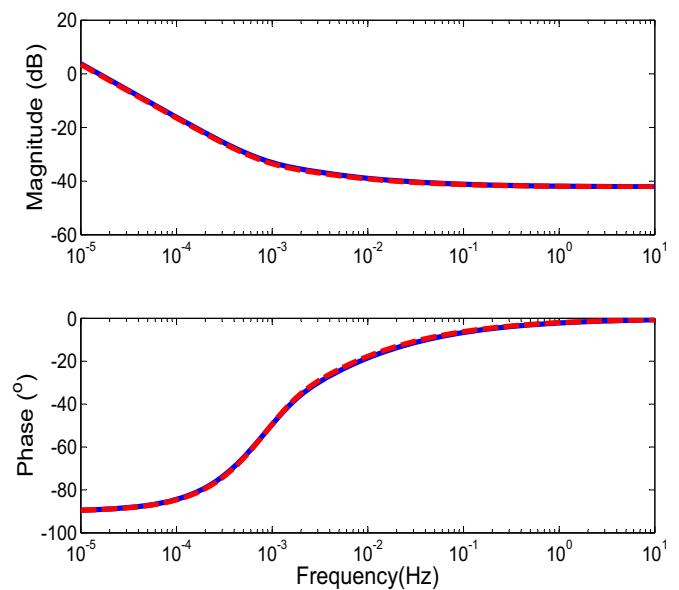$$\frac{V(s)}{I(s)} = \frac{b_3 s^3 + b_2 s^2 + b_1 s + b_0}{s^3 + a_2 s^2 + a_1 s} \qquad (10)$$

Fig. 2. Impedance frequency response: SP model (blue-solid) and SP model with only positive electrode (red-dashed). (For interpretation of the references to color in this figure legend, the reader is referred to the web version of this article.)

The experimental current and voltage signals are passed through identical fourth order filters, represented in state space form by

$$\dot{\mathbf{w}}_1 = \Lambda \mathbf{w}_1 + \mathbf{b}_\lambda I(t), \tag{11}$$

$$\dot{\mathbf{w}}_2 = \Lambda \mathbf{w}_2 + \mathbf{b}_\lambda V(t), \tag{12}$$

where

$$\Lambda = \begin{bmatrix} 0 & 1 & 0 & 0 \\ 0 & 0 & 1 & 0 \\ 0 & 0 & 0 & 1 \\ -\lambda_0 & -\lambda_1 & -\lambda_2 & -\lambda_3 \end{bmatrix}, \quad \mathbf{b}_\lambda = \begin{bmatrix} 0 \\ \vdots \\ 1 \end{bmatrix}. \tag{13}$$

The coefficients $\lambda_0,...,\lambda_3$ are calculated to place the poles of Λ in the left half of the complex plane at a desired filtering speed. The Laplace transform of Eqs. (11) and (12) produces

$$\frac{\mathbf{W}_1(s)}{I(s)} = \frac{1}{s^4 + \lambda_3 s^3 + \lambda_2 s^2 + \lambda_1 s^1 + \lambda_0} \begin{bmatrix} 1 \\ s \\ s^2 \\ s^3 \end{bmatrix}, \tag{14}$$

$$\frac{\mathbf{W}_2(s)}{V(s)} = \frac{1}{s^4 + \lambda_3 s^3 + \lambda_2 s^2 + \lambda_1 s^1 + \lambda_0} \begin{bmatrix} s \\ s^2 \end{bmatrix}, \tag{15}$$

The linear parameterization

$$\mathbf{b}^T \mathbf{W}_1(s) + \mathbf{a}^T \mathbf{W}_2(s) = \Theta^T \mathbf{W}(s), \tag{16}$$

where $\mathbf{b}^T = [b_0,b_1,b_2,b_3]$, $\mathbf{a}^T = [-a_1,-a_2]$, $\Theta^T = [\mathbf{b}^T, \mathbf{a}^T]$, and $\mathbf{W}^T(s) = [\mathbf{W}_1^T(s), \mathbf{W}_2^T(s)]$ is expanded to obtain

$$\Theta^T \mathbf{W}(s) = \frac{b_0 + b_1 s + b_2 s^2 + b_3 s^3}{s^4 + \lambda_3 s^3 + \lambda_2 s^2 + \lambda_1 s^1 + \lambda_0} I(s)$$
$$+ \frac{-a_1 s - a_2 s^2}{s^4 + \lambda_3 s^3 + \lambda_2 s^2 + \lambda_1 s^1 + \lambda_0} V(s). \tag{17}$$

Simplifying the above expression using the impedance transfer function in Eq. (10) we obtain

$$\Theta^T \mathbf{W}(s) = \frac{s^3}{s^4 + \lambda_3 s^3 + \lambda_2 s^2 + \lambda_1 s^1 + \lambda_0} V(s) = Z(s) \tag{18}$$

Therefore we have,

$$\hat{z}(t) = \hat{\Theta}^T \mathbf{w}(t), \tag{19}$$

where $\hat{\Theta}$ is the parameter estimate. The error is defined to be

$$e(t) = z(t) - \hat{z}(t) = z(t) - \hat{\Theta}^T \mathbf{w}(t). \tag{20}$$

The experimental voltage and current data is fed through the filters to produce

$$\mathbf{J} = [\mathbf{w}(0), \mathbf{w}(\Delta t), ..., \mathbf{w}((N_{eval} - 1)t)]. \tag{21}$$

where Δt is the sample time and N_{eval} is the total number of data points. The least squares cost function

$$\mathscr{CF} = \left| z - \hat{\Theta}^T \mathbf{J} \right|^2, \tag{22}$$

so the $\hat{\Theta}$ that minimizes the CF is given by

$$\hat{\Theta}_{ls} = \left[\mathbf{JJ}^T\right]^{-1} \mathbf{Jz}. \tag{23}$$

The six parameters in $\hat{\Theta}_{ls}$ are the coefficients of the transfer function Eq. (10) that best-fit the experimental data in a least squares sense. If the model is accurate then the best-fit coefficients should correspond to a unique set of parameters R_T^+, $\mathscr{C}^+$, τ_D^+ in the transfer function Eq. (9). Equating transfer functions Eqs. (9) and (10) results in six nonlinear equations for the three unknown parameters. The best results were obtained by equating the two highest order coefficients in the numerator to produce $\hat{R}_T^+ = \hat{b}_3$ and $\widehat{\mathscr{C}}^+ = \hat{b}_2 - \hat{a}_2 \hat{b}_3$ and the highest order coefficients in the denominator to produce $\hat{\tau}_D^+ = 189/\hat{a}_2$.

4. Recursive parameter estimation

The least squares approach provides a means of finding the best fit parameters for the SP model using a batch of current/voltage data and off-line processing. For real-time implementation onboard a vehicle, recursive parameter identification continually updates the parameter estimates using the all of the measured the voltage and current data up to and including the current time instant. The estimation loop is run in the battery monitoring control software at a fixed sample rate and continually updates the estimates in real-time. This software is relatively simple and fast to execute, resulting in less burden on the battery monitoring microprocessor. This would be a crucial step prior to adoption in practice.

Fig. 6 shows the block diagram for the gradient based parameter estimator that is proposed for real-time parameter estimation. The objective is to estimate the parameter vector θ^T from the voltage and current data in real-time using a recursive algorithm that continually updates the parameter estimates as information becomes available. The parameter estimator include the input and output filters given by Eqs. (11) and (12), respectively and two gradient update laws

$$\dot{\hat{b}} = \gamma_1 e(t) w_1(t) \tag{24}$$

$$\dot{\hat{a}} = \gamma_2 e(t) w_2(t) \tag{25}$$

that are integrated in real-time to produce the time-varying estimates of the numerator $\hat{\mathbf{b}}(t)$ and denominator $\hat{\mathbf{a}}(t)$ coefficients. The gradient update laws depend on the filtered current and voltage, the error
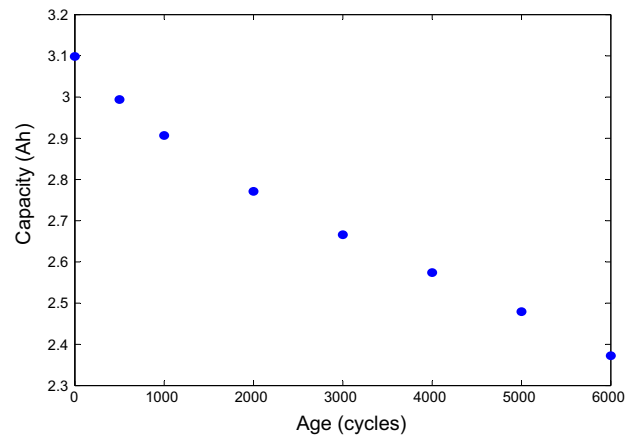

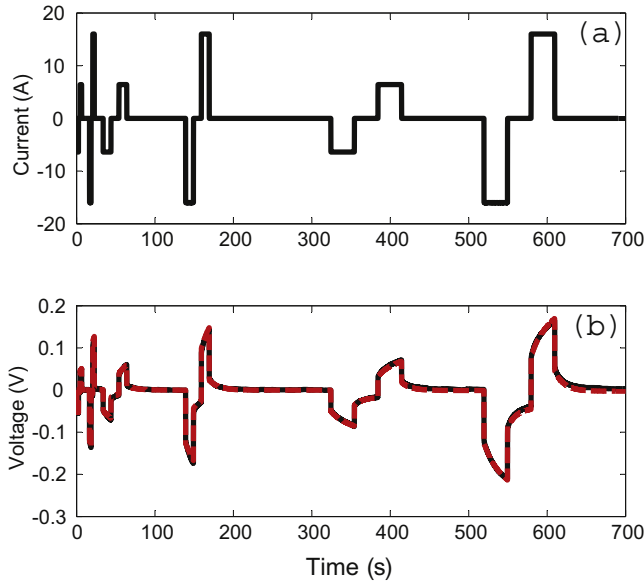Fig. 3. Experimentally measured capacity versus age.

Fig. 4. Pulse charge/discharge response: (a) Input current and (b) measured voltage (black-solid) and fitted model response (red-dashed). (For interpretation of the references to color in this figure legend, the reader is referred to the web version of this article.)

$$e(t) = z(t) - \left(\widehat{\mathbf{b}} w_1(t) + \widehat{\mathbf{a}} w_2(t) \right) \tag{26}$$

and the adaptation gain γ_1 and γ_2.

5. Results and discussion

Seven commercial 3Ah lithium ion cells were cycled continuously at 5C-rate between 3.0 V and 4.2 V at 45 °C on an Arbin BT-2000 battery cycler. This charge/discharge protocol enables accelerated aging. The cycling of the seven cells was terminated after 500, 1000, 2000, 3000, 4000, 5000 and 6000 cycles, respectively. After cycling termination, the capacity, electrochemical impedance spectroscopy (EIS) data, and hybrid pulse power characterization (HPPC) [19] were measured. Fig. 3 shows the measured
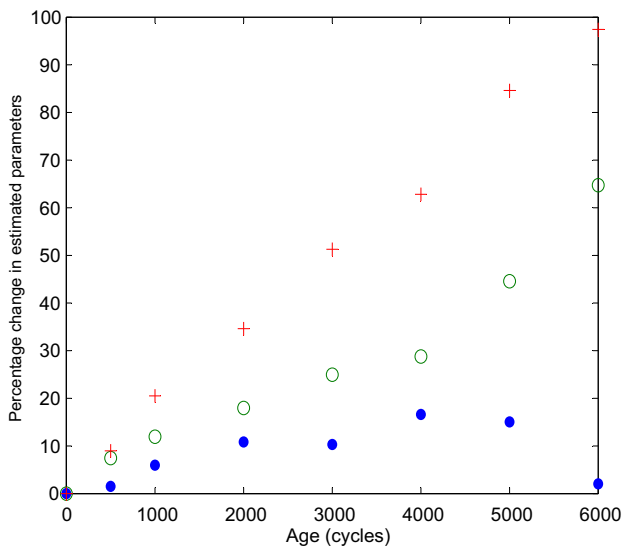

Fig. 5. Estimated resistance ($\widehat{R}_T^+$, +), diffusion time ($\widehat{\tau}_D^+$, o), and capacity factor ($\widehat{C}^+$, •) versus age.

capacity of these aged cells and a fresh cell. The pulse charge/discharge data from the HPPC test was obtained for each of the fresh and aged cells at 60% State of Charge (SOC), C-rates of 2C and 5C for different pulse durations (2s, 10s and 30s), and at 25 °C. Fig. 4 shows the input pulse train and the experimentally measured cell voltage response for the fresh cell. The proposed methodology of SOH estimation from model parameter estimation is based on the following conditions:

- The model parameters must be estimable from real-time measurements of voltage and current. This requires that the model be sufficiently simple with few parameters and the voltage/current data must be sufficiently rich so that the parameters converge close to their actual values. The parameters R_T^+, $\mathscr{C}^+$, τ_D^+ are estimated using the least squares technique from the experimental pulse current and voltage data, demonstrating that they satisfy this condition. Fig. 4 shows the excellent match between the experimental and identified model voltage responses for a fresh cell using the estimated model parameters. The overall response and the peaks/valleys match very well, including the high current and long duration 5C pulses. The SOC only deviates by 4% during these pulses, however, so the linearized OCV assumption applies.
- The SOH or instantaneous capacity of the cell must be related to the model parameters by an invertible function. The SOH as a function of parameter value must be invertible because the parameter will be estimated in real-time and the SOH calculated through this inverse function. The inverse function must be one-to-one so that a given parameter value only results in one possible SOH. Non-invertible functions that do not produce one-to-one results will have multiple possible SOH values for the same parameter value. This may be overcome by tracking the SOH over the life of the cell and using the value closest to the previous value. If the estimator ever "forgets" (e.g. power loss to microprocessor) the previous value, however, then it cannot be recovered. Parameters that vary monotonically with age are excellent candidates for SOH estimation because they are invertible and produce one-to-one inverse functions. The least squares technique is applied to all eight cells and Fig. 5 shows the estimated parameters as functions of age. The total resistance R_T^+ and diffusion time τ_D^+ monotonically increase as the battery ages so they satisfy this condition.
- The aging cycle test data must be representative of actual battery usage. The way a battery ages can depend on usage. The current and temperature inputs must be representative of typical usage. The algorithm should then be validated against extreme cases to determine if the methodology holds up under those conditions. This would be a crucial step prior to adoption in practice.

The monotonic increase in $\widehat{R}_T^+$ as the battery ages is due to an increase in either charge transfer resistance, contact resistance, or both. Charge transfer resistance increase can be explained by the growth of a resistive SEI layer on the active particles of the positive electrode. Contact resistance generally increases with age due to contact loss between the electrode and the current collectors from corrosion. The monotonic increase in $\widehat{\tau}_D^+$ as the battery ages is also consistent with the growth of an SEI layer on the active particles in the positive electrode which would reduce the effective diffusion rate of Li$^+$ ions.

Based on the empirical results in Fig. 5, two possible SOH estimates are

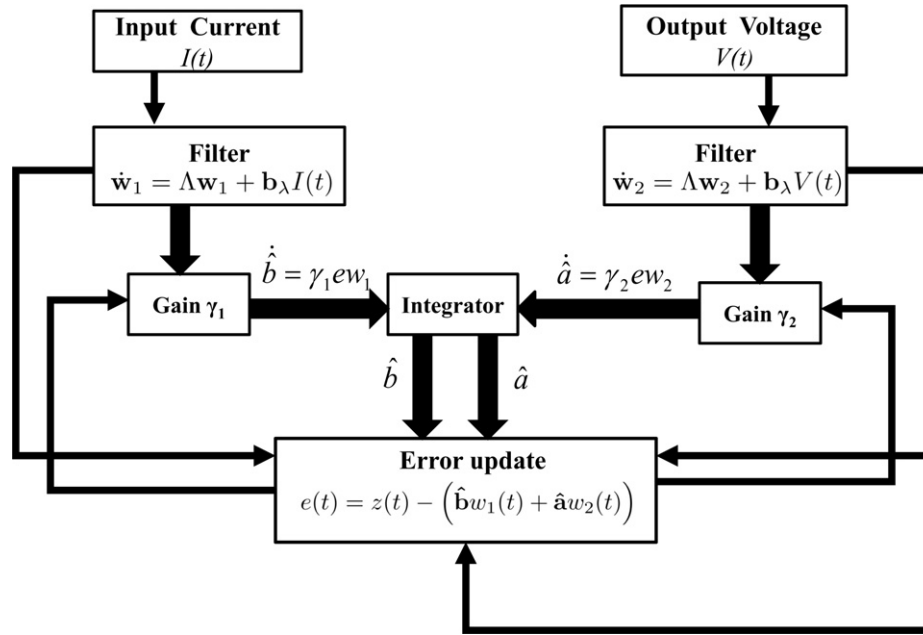$$SO\widehat{H}_{R_T^+}(t) = \frac{\widehat{R}_T^+(t)}{\widehat{R}_T^+(0)} \tag{27a}$$

Fig. 6. Recursive parameter estimator block diagram.

$$SO\widehat{H}_{\tau_D^+}(t) = \frac{\widehat{\tau}_D^+(t)}{\widehat{\tau}_D^+(0)} \tag{27b}$$

Fig. 5 shows that the capacity factor estimate $\widehat{\mathscr{C}}^+$ rises slowly, reaching a maximum of 17% at 4000 cycles and then decreases to 2% at 6000 cycles. This non-monotonic variation renders SOH estimation based on capacity factor impossible because the capacity factor estimate is the same at different ages as shown in Fig. 5. The capacity factor estimate cannot be inverted to infer the capacity because the inverse function is not one-to-one. It is also difficult to physically explain the capacity factor variation with age

in terms of the SEI layer formation degradation mechanism. The capacity factor is a function of the slope of the OCV curve and the electrode volume fraction, so it may be relevant to other battery chemistries, manufacturers, and degradation mechanisms.

To demonstrate the functionality of the recursive parameter estimator discussed in Section 4, the fresh cell voltage and current data is processed in real-time as shown in Fig. 7. In this simulation, all of the coefficients are initialized to their least square, best fit values, except for the coefficients associated with the two SOH indicators, R_T^+ and τ_D^+, which are initialized to 5% of their actual values. The adaptation gains are adjusted to provide fast parameter convergence with minimal oscillation. The current excitation is sufficiently rich to ensure that the parameter estimates converge to within 99% of their least square, best fit values in less than 200 s.

6. Conclusion

A third order, single particle, positive electrode model of lithium ion cells enables the development of least square and recursive parameter estimators. Least square estimates of the composite parameters of total resistance and diffusion time are shown to increase monotonically with age of commercial lithium ion cells that have been charged/discharged at 5C for up to 6000 cycles. This model based parameter estimation scheme helps in developing a correlation between the degradation mechanisms and the battery parameters and provides a foundation for SOH estimation. Increases in the charge transfer resistance and diffusion can be attributed to the growth of a resistive SEI layer on the active particles of the positive electrode. An increase in contact resistance with age is typically associated with contact loss between the electrode and the current collectors. With sufficiently rich (HPPC) current excitation, the total resistance and diffusion time estimates converge to within 99% of their best fit values in 200 s using a gradient parameter update law in real time. The total resistance and diffusion time estimates provide two independent measures of lithium ion battery SOH that can be calculated in real time, on-board a vehicle.
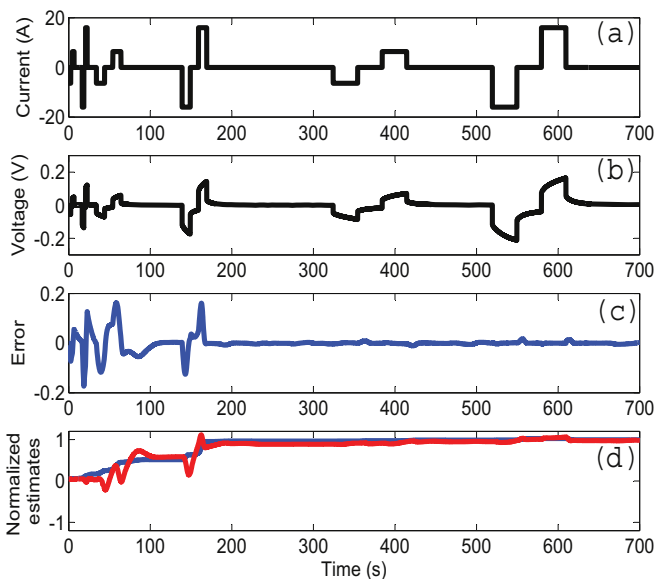

Fig. 7. Gradient based recursive parameter estimation for a fresh cell:(a) Current, (b) Voltage, (c) Error, (d) Normalized parameter estimates (Resistance (blue), Diffusion rate (Red)). (For interpretation of the references to color in this figure legend, the reader is referred to the web version of this article.)

References

[1] D. Zhang, B. Haran, A. Durairajan, R. White, Y. Podrazhansky, B. Popov, Journal of Power Sources 91 (2) (2000) 122–129.

[2] A.T. Stamps, C.E. Holland, R.E. White, E.P. Gatzke, Journal of Power Sources 150 (0) (2005) 229–239.

[3] P. Ramadass, B. Haran, R. White, B.N. Popov, Journal of Power Sources 123 (2) (2003) 230–240.

[4] J. Vetter, P. Novák, M. Wagner, C. Veit, K.-C. Moller, J. Besenhard, M. Winter, M. Wohlfahrt-Mehrens, C. Vogler, A. Hammouche, Journal of Power Sources 147 (2005) 269–281.

[5] M. Doyle, T. Fuller, J. Newman, Journal of the Electrochemical Society 140 (1993) 1526–1533.

[6] K.A. Smith, C.D. Rahn, C.-Y. Wang, Energy Conversion and Management 48 (2007) 2565–2578.

[7] A.P. Schmidt, M. Bitzer, Árpád W. Imre, L. Guzzella, Journal of Power Sources 195 (22) (2010) 7634–7638.

[8] Y. Zhang, C.-Y. Wang, Journal of The Electrochemical Society 156 (7) (2009) A527–A535.

[9] J. Remmlinger, M. Buchholz, M. Meiler, P. Bernreuter, K. Dietmayer, Journal of Power Sources 196 (12) (2011) 5357–5363.

[10] J. Kim, B. Cho, Vehicular Technology, IEEE Transactions on 60 (9) (2011) 4249–4260.

[11] D. Haifeng, W. Xuezhe, S. Zechang, A new SOH prediction concept for the power lithium-ion battery used on HEVs, in: Vehicle Power and Propulsion Conference, 2009, VPPC '09, IEEE, 2009, pp. 1649–1653.

[12] G.L. Plett, Journal of Power Sources 134 (2) (2004) 252–261.

[13] G.L. Plett, Journal of Power Sources 134 (2) (2004) 262–276.

[14] G.L. Plett, Journal of Power Sources 134 (2) (2004) 277–292.

[15] U. Troltzsch, O. Kanoun, H.-R. Trankler, Electrochimica Acta 51 (2006) 1664–1672.

[16] I.-S. Kim, Power Electronics, IEEE Transactions on 25 (4) (2010) 1013–1022.

[17] G.K. Prasad, C.D. Rahn, Development of a first principles equivalent circuit model for a lithium ion battery. Ft. Lauderdale, FL, in: Asme Dynamic Systems and Control Conference, 2012.

[18] J.C. Forman, S. Bashash, J.L. Stein, H.K. Fathy, Journal of The Electrochemical Society 158 (2) (2011) A93–A101.

[19] Y. Zhang, C.-Y. Wang, X. Tang, Journal of Power Sources 196 (3) (2011) 1513–1520.